Coiled-coil registry shifts in the F684I mutant of Bicaudal D result in cargo-independent activation of dynein motility

Heying Cui[1], M. Yusuf Ali[2], Puja Goyal[1], Kaiqi Zhang[1], Jia Ying Loh[1], Kathleen M. Trybus[2], Sozanne R. Solmaz[1,*]

[1]Department of Chemistry, State University of New York at Binghamton, PO Box 6000, Binghamton, NY 13902. [2]Department of Molecular Physiology & Biophysics, University of Vermont, Burlington VT 05405.

Supplemental Materials

Table of Contents **Page**

Supplemental Figures and Movies

Movie S1. Movie showing diffusive motion of dynein-dynactin-BicD WT (DDB^{WT}) on rhodamine-labeled microtubules. The dynein is labeled with a Qdot. Movies are 8x real speed. Horizontal distance, 9.8 μm. Scale bar, 2 μm.

Movie S2. Movie showing processive motion of dynein-dynactin-BicD-CC1 (DDB^{CC1}) on rhodamine-labeled microtubules. The dynein is labeled with a Qdot. Movies are 8x real speed. Horizontal distance, 10.2 μm. Scale bar, 2 μm.

Movie S3. Movie showing processive motion of dynein-dynactin-BicD/F684I (DDB^{F684I}) on rhodamine-labeled microtubules. The dynein is labeled with a Qdot. Movies are 8x real speed. Horizontal distance, 10.3 μm. Scale bar, 2 μm

Table S1. Single molecule motility parameters of dynein-dynactin BicD complexes using two independent protein preparations of full-length BicD.

BicD construct	BicD preparation	n	Normalized binding frequency[a]	n	Run length (µm)	Speed (µm/s)
WT	1	24	0.22 ± 0.04	-	n.d.	n.d.
CC1	1	33	1 ± 0.13	57	2.9 ± 0.10	0.40 ± 0.13
F684I	1	35	0.85 ± 0.12	72	3.3 ± 0.08	0.42 ± 0.17
WT	2	27	0.26 ± 0.03	-	n.d.	n.d.
CC1	1	33	1 ± 0.08	67	3.7 ± 0.23	0.44 ± 0.19
F684I	2	32	0.87 ± 0.07	72	2.5 ± 0.22	0.37 ± 0.20

[a]Binding frequency of DDB^{CC1} is normalized to one and reported as mean ± SE.
n.d., not determined, because motion is mainly diffusive.

Protein preparation 1 data are from Figure 1, the legend of which provides statistics. The second set of data were generated using independent preparations of $BicD^{WT}$, $BicD^{F684I}$, and dynein. Binding frequency of DDB^{CC1} and DDB^{F684I} are similar (p=0.059, one way ANOVA followed by a Tukey's post-hoc test) but significantly different from DDB^{WT} ($p<0.0001$). Speeds of DDB^{CC1} and DDB^{F684I} are not significantly different (p=0.13, Student's t-test). Run lengths of DDB^{CC1} and DDB^{F684I} are not significantly different (p=0.13, Kolmogorov-Smirnov test).

Table S2. Analytical ultracentrifugation of BicD constructs.

		Single species fit	Two species fit			
BicD	prep	Sedimentation coefficient (S)	Sedimentation coefficient (S)	Concentration (OD)	Sedimentation coefficient (S)	Concentration (OD)
WT	1	5.71 ± 0.02	5.60 ± 0.03	0.570± 0.011	9.47 ± 0.18	0.094 ± 0.013
F6841	1	5.64 ± 0.02	5.37 ± 0.01	0.465± 0.013	7.68 ± 0.13	0.244 ± 0.013
WT	2	5.78 ± 0.02	5.77 ± 0.01	0.618 ± 0.004	10.24 ± 0.14	0.029 ± 0.004
F6841	2	5.51 ± 0.02	5.50 ± 0.02	0.753 ± 0.006	9.87 ± 0.26	0.023 ± 0.007

Methods: Buffer: 30 mM HEPES pH 7.5, 300 mM potassium acetate, 2 mM magnesium acetate, 1 mM EGTA, 1 mM DTT, 20°C. Sedimentation velocity runs were performed in an Optima XL-I analytical ultracentrifuge (Beckman Coulter) using an An60Ti rotor at 40,000 rpm. The sedimentation coefficient was determined by curve fitting to one or two species using the d*c*/d*t* program [68]. Related to Figure 1.

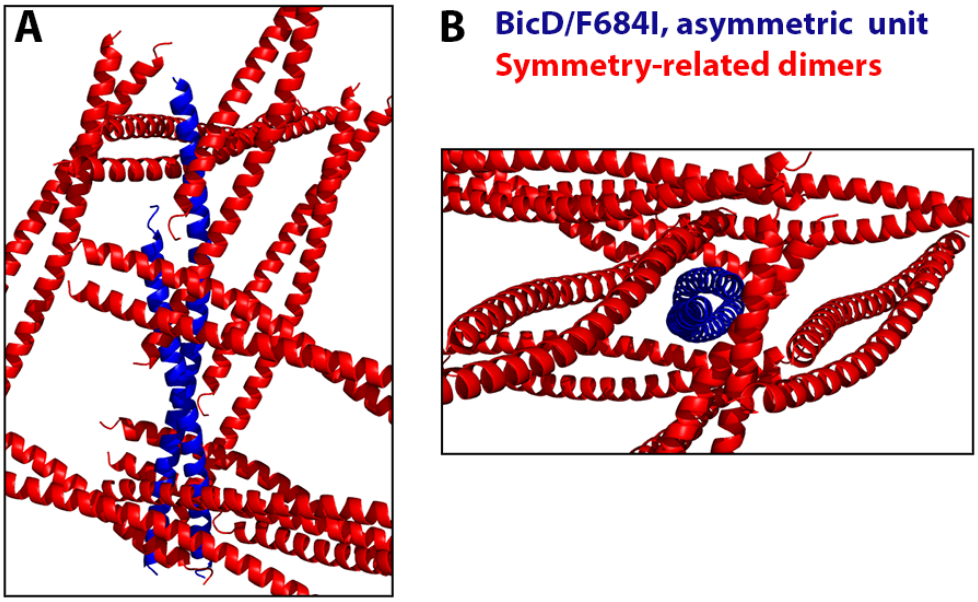

Figure S1. Crystal contacts. (A, B) The structure of the *Dm* BicD-CTD/F684I is shown in cartoon representation; the asymmetric unit is colored blue. To visualize crystal contacts, the symmetry-related dimers from the crystal lattice are shown in red. (B) View from the top of the N-terminus of the asymmetric unit. Related to Figure 2.

(A) Assignment of heptad repeats for *Dm* BicD-CTD/F684I

```
Chain A
MSKLRNELRLLKEDAATISSLRAMFAARCEEYVTQVDDLNRQLEAAEEEKKTLNQLLRLAVQQKLALTQRLEE
Register---------------------------abcdefgabcdefgabcdefgabcdefgabcdefga--
Knobs-----------------------------Y--Y---Y--Y---Y--Y---Y--Y---Y--Y------

Chain B
--------------------LRAMFAARCEEYVTQVDDLNRQLEAAEEEKKTLNQLLRLAVQQKLALTQRLEE
Register---------------------------abcdefgabcdefgabcdefgabcdefgabcdefga--
Knobs---------------X---X-------------X---X--X---X--X---X--X---X--X------
```

(B) Assignment of heptad repeats for *Dm* BicD-CTD (PDB ID 4BL6)

```
Chain A
-----VSDTMSKLRNELRLLKEDAATFSSLRAMFAARCEEYVTQVDDLNRQLEAAEEEKKTLNQLLRLAVQQKLALTQRLEEM
                abcdefgabcdefgabcdefgabcdefgabcdefgabcdefgabcdefgabcdefga
------------Y---Y--Y----------Y-------------Y--Y---Y--Y---Y--Y---Y--Y------Y-------

Chain D
NEKIIVSDTMSKLRNELRLLKEDAATFSSLRAMFAARCEEYVTQVDDLNRQLEAAEEEKKTLNQLLRLAVQQKLALTQRLEEM
     abcdefgabcdefgabcdefgabcdefgabcdefgabcdefgdefgabcdefgabcdefgabcdefgabcdefga
-----X--X---X--X----------X------X-------------X---X--X---X--X---X---------X-------
```

Figure S2. Assignment of heptad repeats for BicD-CTD/F684I. (A, B) The protein sequences from the structures are shown and the Chain IDs from the coordinates are indicated. Y and X denote knob residues that form "knobs-into-holes" interactions with the other chain of the dimer. Knobs-into-holes interactions were identified in the structures with the program SOCKET [60]. A cutoff of 7.5Å and a helix extension of 1 residue were used. Knob residues are denoted by 'Y' and 'X' and are located at 'a' and 'd' positions of the heptad repeat. The unedited output from SOCKET is shown. In Figure 1, all 'a' position residues are shown in sphere representation for which at least one knob was confirmed by SOCKET in a layer. To clarify, if the second 'a' position residue of the layer was not identified as knob by SOCKET, it is still shown in sphere representation, consistent with references [9,10]. See also [30]. For the corresponding figure of *Hs* BicD2-CTD and sequence alignments of *Dm* BicD, *Ms* BicD1 and *Hs* BicD2 see [30]. Related to Figure 2.

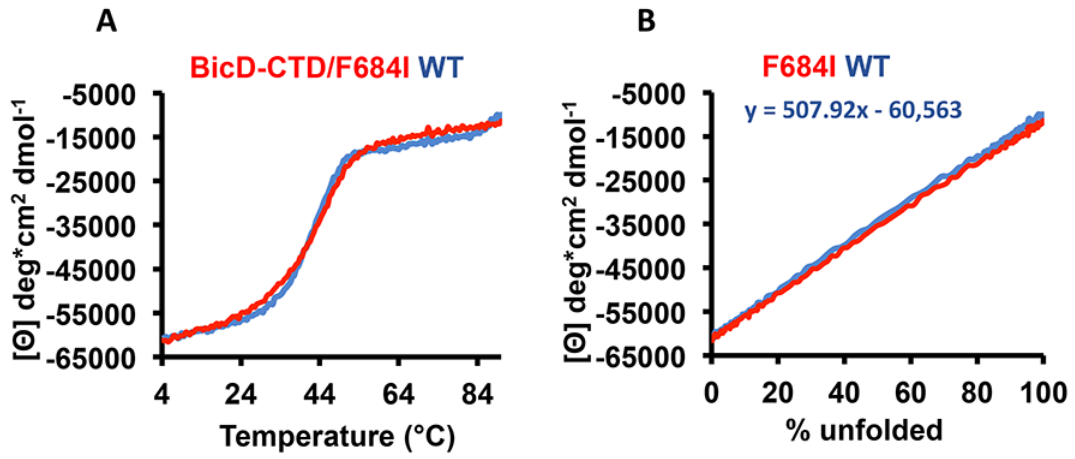

Figure S3. Change of molar ellipticity signal as function of protein unfolding. Related to Figure 4. (A) The same thermal unfolding curves of the wild type (blue) and F684I (red) BicD-CTD as in Figure 4C are shown, but in this representation, the molar ellipticity [Θ] at 222 nm versus the temperature is plotted (instead of % protein unfolded). (B) The molar ellipticity [Θ] versus % protein unfolded is plotted. The equation for the linear trend line for the wild-type curve is shown. A structural change going from 0 - 18% unfolded would result in a change of the molar ellipticity of 9,142 deg*cm^2 dmol^{-1} (a change of 18%). 0% and 100% protein unfolded represent the values of $[\Theta]_{min}$ and $[\Theta]_{max}$, respectively.

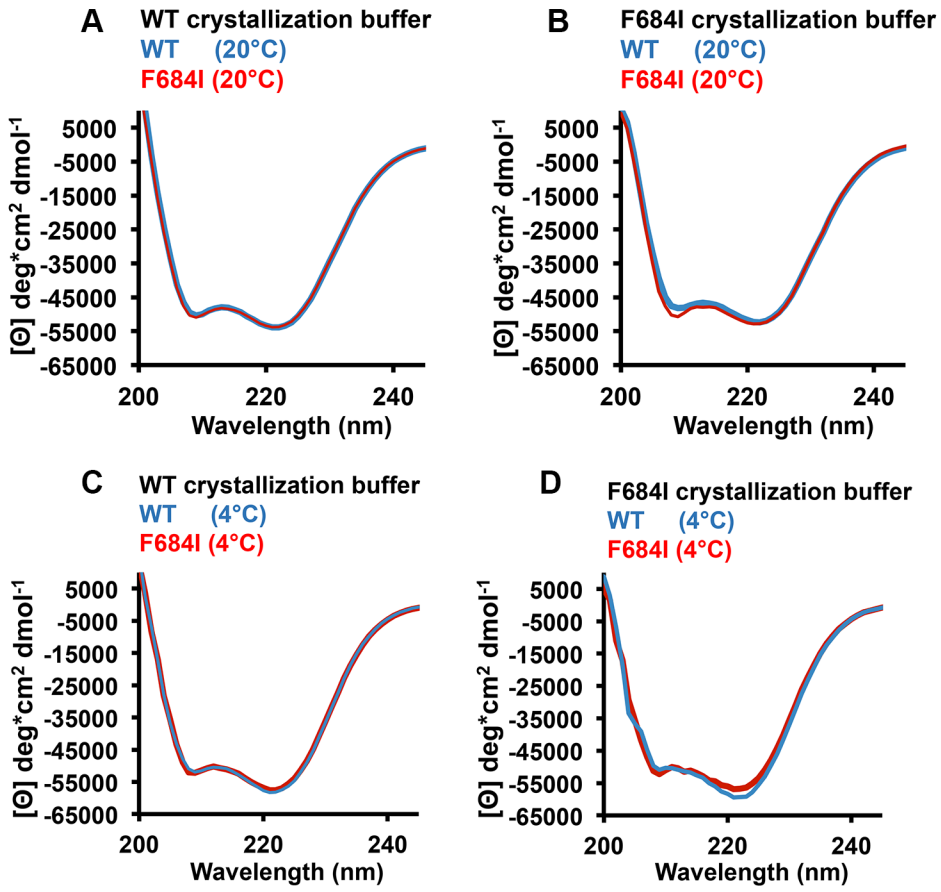

Figure S4. The composition of the crystallization buffers does not affect the α-helical content of *Dm* BicD-CTD WT or the F684I mutant. (A-D) In the structure of the *Dm* BicD-CTD/F684I mutant, a ~20 residue region is disordered, whereas this region is α-helical in the wild-type structure. In order to exclude the possibility that differences in the chemical composition of the WT and F684I mutant crystallization buffers were responsible for the observed structural differences, we recorded CD wavelength scans of *Dm* BicD-CTD WT (blue) and *Dm* BicD-CTD/F684I mutant (red) at (A,B) 20°C (which was the temperature at which crystals were grown) and (C,D) 4°C in (modified) crystallization buffers. The mean residue molar ellipticity [Θ] versus the wavelength is shown. The crystallization buffers were modified for CD spectroscopy in order to reduce the background and to prevent precipitation of the proteins (since the protein solubility is lower in the crystallization buffers). Experiments were repeated twice with similar results, representative experiments are shown. Note that the α-helical content of the *Dm* BicD-CTD WT and F684I proteins is very similar in both crystallization buffers at 20 and 4°C (see also Figure 4B).

Based on these data, it is unlikely that the disorder in the ~20 residue region that is observed in the structure of the *Dm* BicD-CTD/F784I mutant is caused by differences in the chemical composition of the crystallization buffers. Therefore, we conclude that the observed disorder is likely caused by structural flexibility rather than unfolding. Related to Figure 4.

(A, C) CD spectroscopy was performed in the following buffer: 20 mM Tris pH 8.5, 2.5% PEG4000, 15 mM $CaCl_2$, 15 mM $MgCl_2$, 75 mM NaCl, and 0.2 mM TCEP. The following buffer was used for crystallization of the *Dm* BicD-CTD WT: 0.1 M Tris pH 8.5, 5% PEG4000, 30 mM $CaCl_2$, 30 mM $MgCl_2$, 10% glycerol, 10 – 20 mM HEPES pH 7.4, 75 - 150 mM NaCl, and 2.5 - 5 mM β-mercapthoethanol (BME). Crystallization was performed at 18°C [9]. (B, D) CD spectroscopy was performed in the following buffer: 10 mM Tris pH 7.5, 3 mM NaSCN, 150mM NaCl, and 0.2 mM TCEP. The following buffer was used for crystallization of the *Dm* BicD-CTD/F743I mutant: 4% PEG3350, 0.4 M NaSCN, 5 % glycerol, 10-20 mM HEPES pH 7.5, 75-150 mM NaCl, and 0.2-0.5 mM TCEP. Crystallization was performed at 20°C.

Table S3. Dimer interface of crystal structure of *Dm* BicD-CTD/F684I. For the corresponding Table for *Hs* BicD2-CTD see [30].

***Dm* BicD-CTD F684I**			***Dm* BicD-CTD** (PDB ID 4BL6)		
Chain A	Chain B	Dist(Å)	Chain A	Chain D	Dist (Å)
Hydrogen bonds			**Hydrogen bonds**		
TYR 698 OH	CYS 695 SG	3.05	TYR 698 OH	CYS 695 SG	3.2
GLN 701 OE1	TYR 698 OH	2.70	GLN 701 OE1	TYR 698 OH	3.0
LYS 716 NZ	GLU 715 OE1	3.42	GLU 715 OE1	LYS 716 NZ	2.5
ASN 720 ND2	GLU 715 OE2	3.70	ARG 688 NH1	ASP 680 OD1	2.8
			ARG 688 NH2	THR 683 OG1	2.8
Salt bridges			**Salt bridges**		
GLU 715 OE1	LYS 716 NZ	3.37	GLU 715 OE1	LYS 716 NZ	2.5
GLU 715 OE2	LYS 716 NZ	3.29	GLU 715 OE2	LYS 716 NZ	3.9
LYS 716 NZ	GLU 715 OE1	3.42	ARG 688 NH1	ASP 680 OD1	2.8
LYS 716 NZ	GLU 715 OE2	3.90	ARG 688 NH2	ASP 680 OD1	3.1
			LYS 716 NZ	GLU 715 OE2	2.9
Interface area			**Interface area**		
1427 Å^2			1764 Å^2		
Interface residues			**Interface residues**		
684, 685, 687, 688, 691, 694, 695, 698, 701, 702, 705, 706, 708, 709, 712, 713, 715, 716, 719, 720, 722, 723, 725, 726, 727, 729, 730, 733, 734, 736, 737, 740			659, 662, 663, 664, 666, 667, 669, 670, 671, 673, 674, 677, 678, 680, 681, 683, 684, 687, 688, 690, 691, 692, 694, 695, 698, 699, 701, 702, 705, 706, 708, 709, 712, 713, 715, 716, 719, 720, 722, 723, 726, 727, 729, 730, 733, 734, 736, 737, 740		

Standard nomenclature from the structure coordinates is used for Chain ID, residue and atom names. Dist: Distance. Analysis was performed with the PISA server [61]. Related to Figure 4.

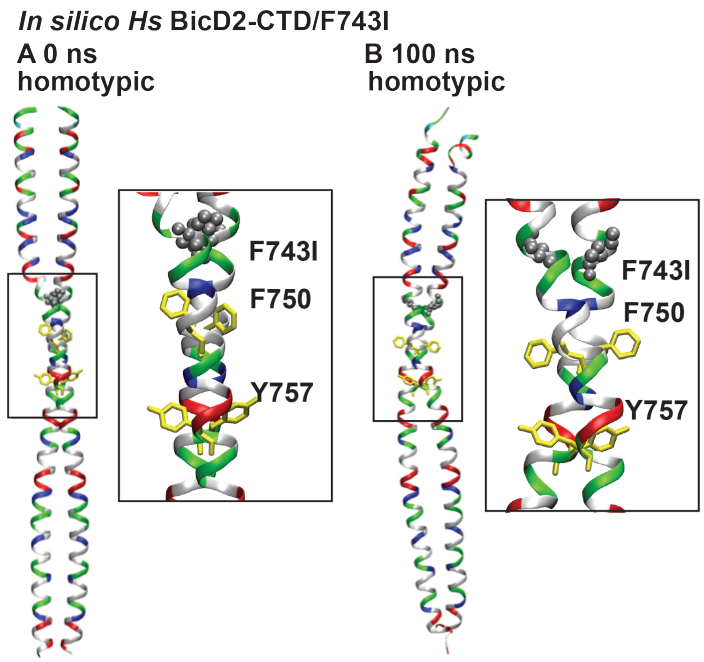

Figure S5. MD simulations suggest that the human BicD2-CTD/F743I mutant can assume a conformation with a homotypic coiled-coil registry. For these simulations, the structure of *Hs* BicD2-CTD was chosen as a starting point, since it has a homotypic coiled-coil registry, [30] and the homologous F743I mutation was introduced. **(**A) Cartoon representation of the crystal structure of human BicD2-CTD,[30] with homotypic registry, colored by residue type (blue: positively charged, red: negatively charged, green: polar, white: non-polar). F743 was mutated to isoleucine (silver spheres). F750 and F757 are shown in yellow stick representation. A close-up of the boxed area is shown on the right. (B) Equilibrated structure of the F743I mutant of human BicD2-CTD at the end of a 100 ns MD simulation. Note that in these MD simulations, the homotypic registry of the *Hs* BicD2-CTD/F743I was preserved, suggesting that the mutant can assume a conformation with a homotypic registry. In comparison, in our recent MD simulations of *Hs* BicD2-CTD/F743I with asymmetric coiled-coil registry, the F743I mutation induced a coiled-coil registry shift from an asymmetric to a fully heterotypic registry.[30] Results from these simulations combined support the idea that the human homolog of the F684I mutant (i.e. F743I) can also sample conformations with distinct coiled-coil registries, likely resulting in conformational flexibility.

Related to Figure 5. The structure coordinate files that were used to create Figure 5 and Figure S5 are available on Dr. Puja Goyal's laboratory website as File S1.